Title
Resonantly Enhanced Electromigration Forces for Adsorbates on Graphene

Journal
Physical Review Letters, 129(20)

ISSN
0031-9007

Authors
Choi, Young Woo
Cohen, Marvin L

Publication Date
2022-11-11

DOI
10.1103/physrevlett.129.206801

Peer reviewed

Resonantly Enhanced Electromigration Forces for Adsorbates on Graphene

Young Woo Choi and Marvin L. Cohen*
Department of Physics, University of California, Berkeley, California 94720, USA
and Materials Sciences Division, Lawrence Berkeley National Laboratory, Berkeley, California 94720, USA

We investigate the electromigration forces for weakly bonded adsorbates on graphene by using density-functional based calculations. We find that the nature of electromigration forces on an adsorbate critically depends on the energy level alignment between the adsorbate state and the Fermi level of the graphene. For a resonant adsorbate, whose frontier orbitals lie close to the Fermi level, the electromigration force is dominated by the electron wind force that is strongly enhanced along the electron flow direction, irrespective of the sign of the adsorbate charge. For a nonresonant adsorbate, the electromigration force is essentially the direct force that depends on the adsorbate charge. We also show that the magnitude of electromigration forces can be continuously tunable through electrostatic gating for resonant adsorbates. Our results provide new insight for understanding and controlling how nanoscale objects behave in or on host materials.

Surface functionalization of graphene through atomic and molecular adsorbates offers a highly effective way to control the electronic and transport properties of graphene [1–3]. Among various adsorbates, tetrafluoro-tetracyanoquinodimenthane (F_4TCNQ), a well-known electron acceptor when placed on graphene [4,5], is particularly interesting because it displays a plethora of intriguing atomic-scale behaviors such as molecular self-assembly, correlation effects, and molecular shift register [6–8]. In addition, a recent experiment has demonstrated that the spatial arrangement and concentration of F_4TCNQ adsorbates can be reversibly controlled by electrical gating [9].

Electromigration is the movement of atoms arising from electrical currents [10]. It provides a convenient way to electrically control the position of atoms or nanoscrystals in nanostructures. In particular, current-induced motion of various metallic nanocrystals in carbon nanotubes has been intensively investigated [11–14]. Also, electromigration of Al and Au clusters on graphene has been observed [15]. Previous theoretical studies focused on the electromigration mechanism for a static potential scatterer and pointed out the dominant role of the electron wind force arising from impurity scattering [16,17]. However, a resonant scatterer, such as F_4TCNQ, has a highly energy-dependent impurity scattering strength [18], and its role on the electromigration mechanism was not addressed in the previous studies.

In this Letter, we investigate electromigration forces for weakly bonded adsorbates on graphene by using density functional theory combined with a nonequilibrium Green's function formalism (DFT-NEGF). We consider three kinds of adsorbates: F_4TCNQ, tetrathiafulvalene (TTF), and atomic Cs [4,19]. F_4TCNQ and TTF are resonant adsorbates whose orbital energy levels are close to the Fermi level. They show strong electromigration forces in the electron flow direction. In this case, the force direction does not depend on the sign of the adsorbate charge. In contrast, an atomic Cs only feels a weak direct force related to its charge. For resonant adsorbates, we show that the magnitude of the electromigration force can be continuously controlled by tuning the position of the Fermi level relative to the resonance energy via electrostatic gating.

First, we investigate the electronic structure of graphene with an adsorbate by performing pseudopotential density functional calculations as implemented in SIESTA [20]. We use the VV10 nonlocal van der Waals functional [21], norm-conserving pseudopotentials, and a localized pseudoatomic orbital basis [22]. A real-space mesh cutoff of 500 Ry is used. We employ a 7×7 supercell of graphene with a single adsorbate. The supercell is 25 Å thick along the vacuum direction. The supercell Brillouin zone is sampled by a $3 \times 3 \times 1$ k-point grid and the Fermi-Dirac smearing function is used with the electronic temperature of 300 K. We optimize atomic positions until the force on each atom is less than 0.01 eV/Å.

Figures 1(a), 1(c), and 1(e) show the local atomic structure of a single F_4TCNQ, TTF, and Cs adsorbate on graphene, respectively. We choose the most energetically favorable adsorption site for each case. The electronic structure calculations show that the lowest unoccupied molecular orbital (LUMO) of F_4TCNQ is 0.25 eV below, and the highest occupied molecular orbital (HOMO) of TTF 0.15 eV above the Dirac point energy of graphene [Figs. 1(b) and 1(d)]. Consequently, F_4TCNQ and TTF induces hole and electron doping to graphene, respectively.

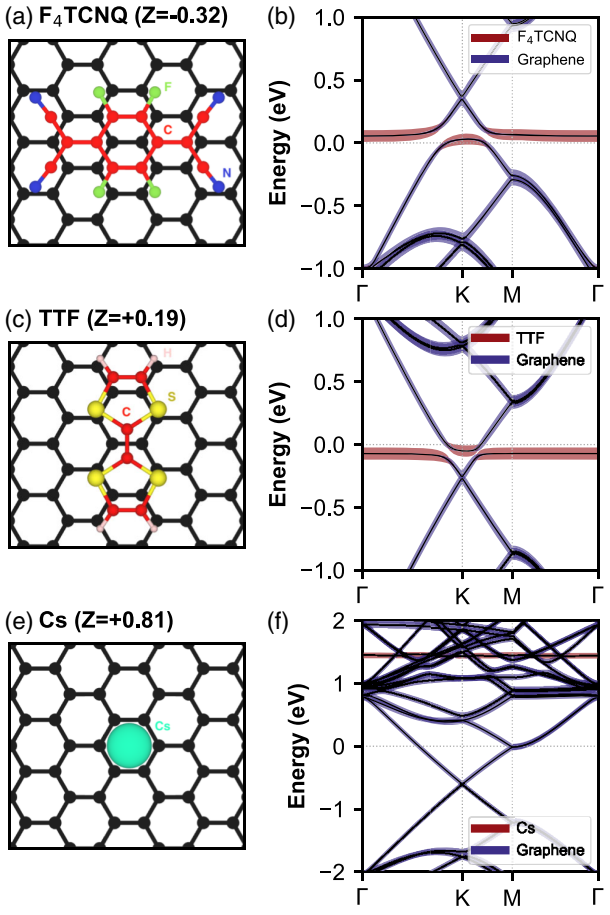

FIG. 1. Atomic structure of graphene with a single (a) F_4TCNQ, (c) TTF, and Cs adsorbate placed at the most stable adsorption site on graphene. The charge Z of the adsorbate is calculated as the sum of the net atomic charges. Electronic structure of graphene with a (b) F_4TCNQ, (d) TTF, and (f) Cs adsorbate. The weight of the orbitals on the adsorbate (graphene) is represented by the thickness of red (blue) lines. The adsorbates F_4TCNQ and TTF have their LUMO and HOMO energy levels very close to the Fermi level, while the $6s$ level of Cs is about 1.4 eV above the Fermi level.

Importantly, the adsorbate states lie very close to the Fermi level of the system, so both molecules act as a resonant impurity [18,23]. In contrast, Fig. 1(f) shows that the $6s$ state of Cs is located far above the Fermi level.

Now, we investigate the current-induced electromigration forces on the adsorbates. The electromigration force is usually analyzed in terms of the direct force and wind force, although this decomposition is not necessarily always rigorous because some ambiguities exist in the definition of adsorbate charge [10]. The direct force is denoted as $\mathbf{F}_d = eZ\mathbf{E}_{\text{ext}}$, where $e > 0$ is the elementary charge, Z is the net charge of an adsorbate, and $\mathbf{E}_{\text{ext}}$ is an external electric field. Hence its direction depends on the sign of adsorbate charge. On the other hand, the wind force $\mathbf{F}_w$ arises from the scattering by the current-carrying electrons, thus the direction of the wind force is in the direction of the net electron flow, which is schematically indicated in Fig. 2(a).

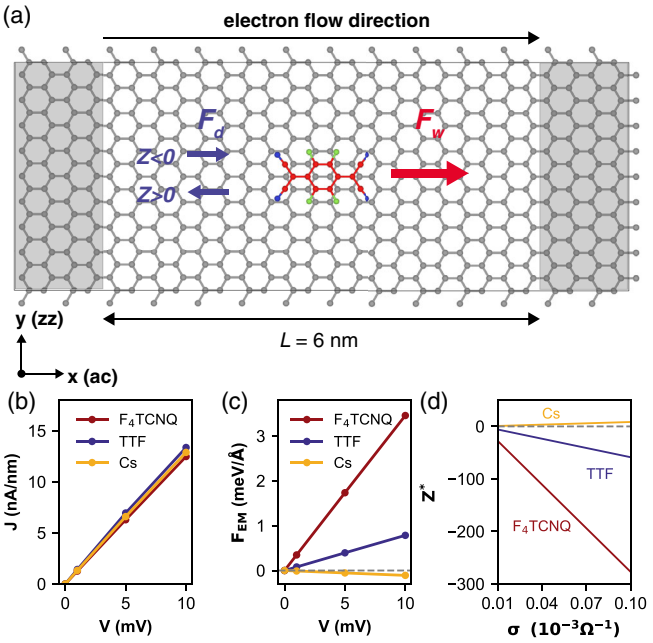

FIG. 2. (a) Two-electrode setup for our NEGF calculations. The device region at the center contains a single adsorbate on graphene, where F_4TCNQ is shown as an example. The left and right gray regions are electrode regions consisting of pristine graphene. The net electron flow is from the left to right, and is along the armchair (x) axis of graphene. Accordingly, the electron wind force is in the $+x$ direction. The direction of the direct force depends on the sign of the adsorbate charge, so it is in the $-x$ ($+x$) direction if $Z > 0$ ($Z < 0$). (b) Electron current densities and (c) total electromigration forces for each adsorbate as a function of the applied bias V. (d) Effective charges for electromigration as a function of graphene bulk conductivity σ.

To self-consistently calculate charge density and electromigration forces under a finite bias, we perform two-electrode DFT-NEGF calculations as implemented in TranSIESTA [24,25]. Figure 2(a) shows the atomic structure for our NEGF calculations with a F_4TCNQ adsorbate as an example [26]. The center scattering region contains an adsorbate on graphene, and we use pristine graphene as the left and right electrode. The system is periodically repeated in the y direction, which is along the zigzag direction of graphene. We sample three k points along the y direction, and 50 points along the x direction in the bulk electrode calculations. A finite bias voltage V is applied across the scattering region by raising (lowering) the chemical potential of the left (right) electrode by $eV/2$. Consequently, the net flow of electrons is along the $+x$ direction. Then, we calculate the electron current density $\mathbf{J}$ from the transmission probability [24,25]. Figure 2(b) shows the calculated electron current densities for each adsorbate. For all three adsorbates, a similar amount of electron current flows through the scattering region. In our calculations, the

current flows through graphene and passes through the adsorbate as well.

In the DFT-NEGF calculation, the electronic contribution to the force on the ith atom located at $\mathbf{R}_i$ is given by

$$\mathbf{F}_i(V) = -\mathrm{Tr}\left[\hat{\rho}(V)\frac{\partial \hat{H}(V)}{\partial \mathbf{R}_i}\right], \tag{1}$$

where $\hat{H}(V)$ is the electronic Hamiltonian, and $\hat{\rho}(V)$ is the electronic density matrix at a finite bias V [24,25,27]. At a given bias, the current-induced nonequilibrium part of the atomic force is given by $\mathbf{F}_{\mathrm{neq},i}(V) = \mathbf{F}_i(V) - \mathbf{F}_i(V=0)$ [28,29]. Then, we obtain the electromigration force on the adsorbate by summing the nonequilibrium forces on the atoms that belong to the adsorbate:

$$\mathbf{F}_{\mathrm{EM}}(V) = \sum_{i \in \text{adsorbate}} \mathbf{F}_{\mathrm{neq},i}(V). \tag{2}$$

Figure 2(c) shows the electromigration forces on the adsorbates along the transport direction. We find that the forces are linearly proportional to the applied bias in this low-bias regime. Interestingly, both F_4TCNQ and TTF show strong electromigration forces along the electron flow direction, in contrast to Cs where the force is an order of magnitude weaker and in the opposite direction.

The strength of electromigration forces can be characterized by an effective charge Z^* defined as $\mathbf{F}_{\mathrm{EM}} = eZ^*\mathbf{E}_{\mathrm{ext}} = -eZ^*\mathbf{J}/\sigma$, where $\mathbf{E}_{\mathrm{ext}} = -\mathbf{J}/\sigma$ is the bulk electric field required to generate the electron current density $\mathbf{J}$ through the channel, and σ is the bulk conductivity of graphene. Figure 2(d) shows the effective charges of the adsorbates as a function of graphene conductivity. Although F_4TCNQ and TTF have the opposite sign of adsorbate charges [Figs. 1(c) and 1(c)], they both have large negative effective charges. This clearly indicates the electromigration force is dominated by the wind force arising from strong impurity scatterings. In contrast, the effective charge of Cs has the same sign as the real charge, and it is an order of magnitude smaller than that for the resonant adsorbates. This means the wind force is ineffective for Cs and the direct force is dominant.

Microscopically, the wind force can be related to the current-induced electron density variations near the adsorbate [10,29,30]. Within the DFT-NEGF, a low-bias expression for the wind force can be derived [29]

$$\mathbf{F}_{w,i} = -\left[\int \delta\rho(\mathbf{r})\nabla_{\mathbf{R}_i} v^l(\mathbf{r})d\mathbf{r} + \sum_{jk}\delta\rho_{jk}\langle\phi_j|\nabla_{\mathbf{R}_i} v^{nl}_{ps}|\phi_k\rangle\right], \tag{3}$$

where $\delta\rho(\mathbf{r})$ is the current-induced changes in the valence electron number density, $\nabla_{\boldsymbol{R}_i} v^l(\mathbf{r})$ and $\nabla_{\boldsymbol{R}_i} v^{nl}_{ps}$ is the gradient of the local part of DFT potential and nonlocal part of the pseudopotential, respectively, and ϕ_i is the pseudoatomic orbital basis for electron wave functions.

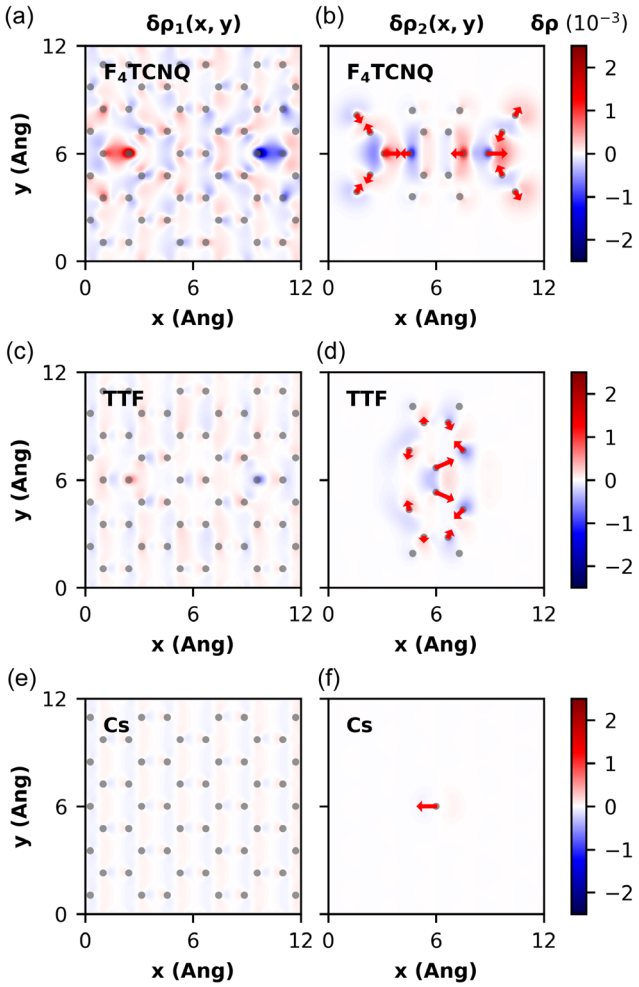

FIG. 3. Current-induced electron number density variations at $V = 10$ mV on (a), (c), (e) graphene ($\delta\rho_1$) and (b), (d), (f) adsorbates ($\delta\rho_2$). $\delta\rho_{1,2}$ is integrated along the z axis within ± 1.5 Å from the graphene plane and the average z position of the adsorbates, respectively. The red arrows on the right figures indicate the current-induced forces on each atom.

This expression provides a microscopic understanding of the electron wind force. First, the current-induced density variations can be conceptually divided into two components ($\delta\rho = \delta\rho_1 + \delta\rho_2$). When electrons are flowing from the left ($-x$) to right ($+x$), the adsorbate scatters incoming electrons resulting in surplus negative charges piled up on the left side of the adsorbate ($\delta\rho_1$), which corresponds to the Landauer dipole [31]. Then, the internal electron density of the adsorbate is redistributed in a screening response to the Landauer dipole in the opposite direction. Thus, the adsorbate is polarized in such a way that there are slightly more electrons on the right side ($\delta\rho_2$). Then, the positively charged core ion, which consists of the nucleus and core electrons, feels an electrostatic force toward the right direction, which is a wind force.

Figure 3 shows the current-induced valence electron density variations $\delta\rho(V) = \rho(V) - \rho(V=0)$ in the real

space for each adsorbate. Here, $\delta\rho_{1,2}(x,y)$ is obtained by integrating $\delta\rho(\boldsymbol{r})$ along the z direction within ± 1.5 Å around the graphene layer and the average z position of the adsorbate, respectively. We interpret $\delta\rho_1$ as the Landauer's dipole formed in the graphene plane, where the incoming and reflected electrons are piled up on the left side of the adsorbate. On the other hand, $\delta\rho_2$ is essentially a screening response of the electrons in the adsorbate against $\delta\rho_1$ in a sense that the overall direction of polarization of $\delta\rho_2$ is opposite to that of $\delta\rho_1$. Since $\delta\rho_2$ is spatially closer to the adsorbate atoms than $\delta\rho_1$, $\delta\rho_2$ plays the dominant role for the wind force [Eq. (3)].

F_4TCNQ and TTF show sizable $\delta\rho_2$, and the directions of the current-induced forces on each atom in the adsorbate are directed toward the nearby regions where there are more electrons. The difference in the magnitude of $\delta\rho_{1,2}$ between F_4TCNQ and TTF stems from their different impurity scattering potential strength and molecular polarizability. Our calculation shows that the F_4TCNQ molecule has about three times higher molecular polarizability than TTF. In contrast, an atomic Cs shows an order of magnitude weaker $\delta\rho$ [Figs. 3(e) and 3(f)]. The total electromigration force is in the left direction, indicating that it is dominated by the electrostatic direct force.

Now, we calculate the electromigration forces for resonant adsorbates under different gating levels. To simulate electrostatic gating, we use the field-effect gate model [32]. In this method, we introduce gate-induced carriers by changing the total number of electrons in the system and placing a uniformly charged plane with the opposite charge to the carriers. The charged plane is put 10 Å below the graphene layer, and the gate-induced carrier density is denoted as n, where $n>0$ ($n<0$) refers to hole (electron) doping.

For neutral ($n=0$) graphene, the frontier orbital energy of F_4TCNQ (TTF) is located right above (below) the Fermi level [Figs. 1(b) and 1(d)]. We can tune the Fermi level of the system by introducing gate-induced carriers on graphene. In our gate-dependent NEGF calculations, we consider F_4TCNQ and TTF on hole-doped ($n>0$) and electron-doped ($n<0$) graphene, respectively. We do not consider other doping configurations because the delocalization error in the approximate exchange-correlation functionals in DFT prevents the molecular orbitals from being fully filled or emptied. For example, when we try to calculate F_4TCNQ on electron-doped ($n<0$) graphene the LUMO of F_4TCNQ is always pinned slightly above the Fermi level and it is pushed up in energy as the Fermi level is increased by gating. This is clearly contrary to experimental situations where the Fermi level can be tuned above the LUMO. We expect that such errors can be partially remedied by employing correction methods to reduce delocalization errors [33,34] and improve level alignments [35], which we leave for future studies.

Figures 4(a) and 4(c) show the electromigration forces for F_4TCNQ and TTF, respectively, under varying gating

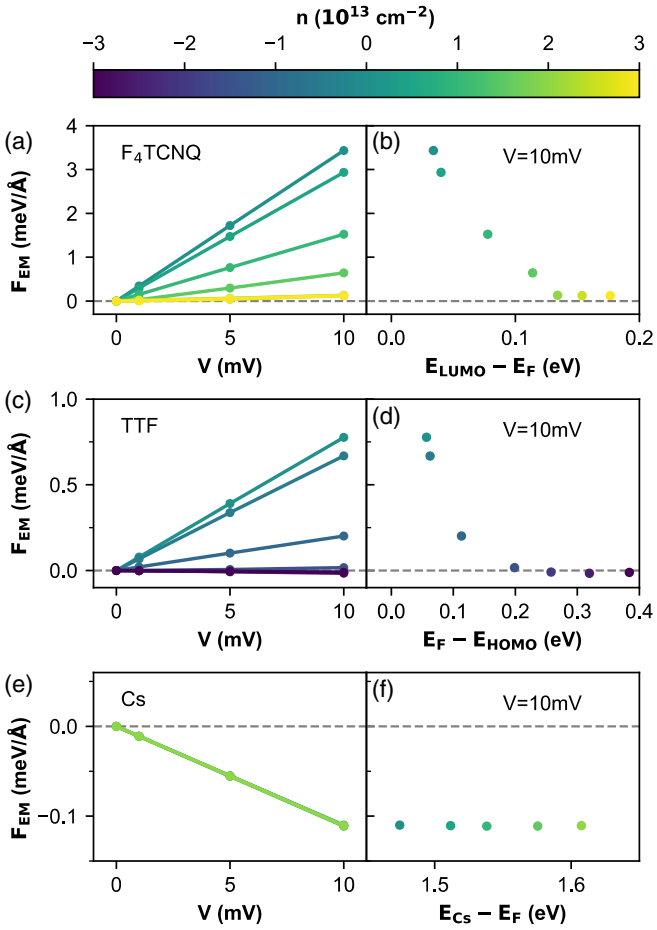

FIG. 4. Gate-dependent electromigration forces for (a) F_4TCNQ, (c) TTF, and (e) Cs on graphene, where $n>0$ ($n<0$) indicates that graphene has additional gate-induced hole (electron) carriers. Here, n is varied from 0 to $\pm 3\times 10^{12}$ cm^{-2} by a step of $\pm 0.5\times 10^{12}$ cm^{-2} for F_4TCNQ and TTF, respectively, and to 2×10^{12} cm^{-2} for Cs. (b),(d),(f) Electromigration forces at $V=10$ mV as a function of the energy difference between the Fermi level of graphene and the resonance orbital energies.

levels. For both cases, the electromigration forces are suppressed as the gating level increases. In Figures 4(b) and 4(d), we show the electromigration forces as a function of the energy difference between the resonance and the Fermi level. As the Fermi level is tuned away from the resonance orbital energies, the electromigration forces are rapidly suppressed. At around $n=2\times 10^{13}$ cm^{-2} for F_4TCNQ and $n=-2\times 10^{13}$ cm^{-2} for TTF, the forces become comparable to the direct forces estimated from their adsorbate charges. In particular, the electromigration force direction for F_4TCNQ remains positive and that for TTF becomes negative at high gating levels, which is expected for the direct force. In contrast, the electromigration force for Cs does not show resonant behavior [Figs. 4(e) and 4(f)]. These results demonstrate that the nature of electromigration forces depends sensitively on the energy level alignment.

To summarize, we have investigated the electromigration forces that acted upon adsorbates on graphene. We have shown that the electron wind force is strongly enhanced along the electron flow direction in the case of resonant adsorbates, and, in contrary, nonresonant adsorbates have a weak direct force. The electron wind force is closely related to the microscopic charge density polarizations near the adsorbates, which is induced as a result of screening the Landauer's dipole. Furthermore, we have demonstrated that the resonant electromigration force can be suppressed by tuning the Fermi level away from the resonance energy. Our results illustrate the crucial role of the energy level alignment of adsorbates on the electromigration mechanism and provide a fundamental understanding on controlling motions of adsorbates on graphene using macroscopic electric fields.

We thank Michael F. Crommie, Hsin-Zon Tsai, and Franklin Liou for helpful discussions. This work was supported primarily by the Director, Office of Science, Office of Basic Energy Sciences, Materials Sciences and Engineering Division, of the U.S. Department of Energy under Contract No. DE-AC02-05-CH11231, within the Theory of Materials program (KC2301), which supported the structural optimization and electronic structure calculations. Further support was provided by the NSF Grant No. DMR-1926004, which supported the finite-bias quantum transport calculations. Computational resources used were Cori at National Energy Research Scientific Computing Center (NERSC), which is supported by the Office of Science of the U.S. Department of Energy under Contract No. DE-AC02-05-CH11231, Stampede2 at the Texas Advanced Computing Center (TACC) through Extreme Science and Engineering Discovery Environment (XSEDE), which is supported by National Science Foundation (NSF) under Grant No. ACI-1053575, Frontera at TACC, which is supported by NSF Grant No. OAC-1818253, and Bridges-2 at the Pittsburgh Supercomputing Center (PSC), which is supported by NSF Award No. ACI-1928147.

*mlcohen@berkeley.edu

[1] T. Ohta, A. Bostwick, T. Seyller, K. Horn, and E. Rotenberg, Controlling the electronic structure of bilayer graphene, Science **313**, 951 (2006).

[2] F. Schedin, A. K. Geim, S. V. Morozov, E. W. Hill, P. Blake, M. I. Katsnelson, and K. S. Novoselov, Detection of individual gas molecules adsorbed on graphene, Nat. Mater. **6**, 652 (2007).

[3] J.-H. Chen, C. Jang, S. Adam, M. S. Fuhrer, E. D. Williams, and M. Ishigami, Charged-impurity scattering in graphene, Nat. Phys. **4**, 377 (2008).

[4] W. Chen, S. Chen, D. C. Qi, X. Y. Gao, and A. T. S. Wee, Surface transfer *p*-type doping of epitaxial graphene, J. Am. Chem. Soc. **129**, 10418 (2007).

[5] C. Coletti, C. Riedl, D. S. Lee, B. Krauss, L. Patthey, K. von Klitzing, J. H. Smet, and U. Starke, Charge neutrality and band-gap tuning of epitaxial graphene on SiC by molecular doping, Phys. Rev. B **81**, 235401 (2010).

[6] H.-Z. Tsai *et al.*, Molecular self-assembly in a poorly screened environment: F_4TCNQ on graphene/BN, ACS Nano **9**, 12168 (2015).

[7] S. Wickenburg *et al.*, Tuning charge and correlation effects for a single molecule on a graphene device, Nat. Commun. **7**, 13553 (2016).

[8] H.-Z. Tsai *et al.*, A molecular shift register made using tunable charge patterns in one-dimensional molecular arrays on graphene, Nat. Electron. **3**, 598 (2020).

[9] F. Liou *et al.*, Imaging reconfigurable molecular concentration on a graphene field-effect transistor, Nano Lett. **21**, 8770 (2021).

[10] R. S. Sorbello, *Theory of electromigration*, in *Solid State Physics* (Elsevier, New York, 1998), Vol. 51, pp. 159–231.

[11] B. C. Regan, S. Aloni, R. O. Ritchie, U. Dahmen, and A. Zettl, Carbon nanotubes as nanoscale mass conveyors, Nature (London) **428**, 924 (2004).

[12] C. Jin, K. Suenaga, and S. Iijima, Plumbing carbon nanotubes, Nat. Nanotechnol. **3**, 17 (2008).

[13] D. Golberg, P. M. F. J. Costa, M. Mitome, S. Hampel, D. Haase, C. Mueller, A. Leonhardt, and Y. Bando, Copper-filled carbon nanotubes: Rheostatlike behavior and femtogram copper mass transport, Adv. Mater. **19**, 1937 (2007).

[14] S. Coh, W. Gannett, A. Zettl, M. L. Cohen, and S. G. Louie, Surface atom motion to move iron nanocrystals through constrictions in carbon nanotubes under the action of an electric current, Phys. Rev. Lett. **110**, 185901 (2013).

[15] A. Barreiro, R. Rurali, E. R. Hernández, and A. Bachtold, Structured graphene devices for mass transport, Small **7**, 775 (2011).

[16] S. Heinze, N.-P. Wang, and J. Tersoff, Electromigration Forces on Ions in Carbon Nanotubes, Phys. Rev. Lett. **95**, 186802 (2005).

[17] D. Solenov and K. A. Velizhanin, Adsorbate Transport on Graphene by Electromigration, Phys. Rev. Lett. **109**, 095504 (2012).

[18] T. O. Wehling, M. I. Katsnelson, and A. I. Lichtenstein, Adsorbates on graphene: Impurity states and electron scattering, Chem. Phys. Lett. **476**, 125 (2009).

[19] H. Akiyoshi, H. Goto, E. Uesugi, R. Eguchi, Y. Yoshida, G. Saito, and Y. Kubozono, Carrier accumulation in graphene with electron donor/acceptor molecules, Adv. Electron. Mater. **1**, 1500073 (2015).

[20] J. M. Soler, E. Artacho, J. D. Gale, A. García, J. Junquera, P. Ordejón, and D. Sánchez-Portal, The SIESTA method for ab initio order-*N* materials simulation, J. Phys. Condens. Matter **14**, 2745 (2002).

[21] O. A. Vydrov and T. Van, Voorhis, Nonlocal van Der Waals density functional: The simpler the better, J. Chem. Phys. **133**, 244103 (2010).

[22] J. Oroya, A. Martín, M. Callejo, M. García-Mota, and F. Marchesin Pseudopotential and Numerical Atomic Orbitals Basis Dataset, provided by SIMUNE Atomistics, www.simuneatomistics.com.

[23] T. O. Wehling, S. Yuan, A. I. Lichtenstein, A. K. Geim, and M. I. Katsnelson, Resonant Scattering by Realistic Impurities in Graphene, Phys. Rev. Lett. **105**, 056802 (2010).
[24] M. Brandbyge, J.-L. Mozos, P. Ordejón, J. Taylor, and K. Stokbro, Density-functional method for nonequilibrium electron transport, Phys. Rev. B **65**, 165401 (2002).
[25] N. Papior, N. Lorente, T. Frederiksen, A. García, and M. Brandbyge, Improvements on non-equilibrium and transport green function techniques: The next-generation transiesta, Comput. Phys. Commun. **212**, 8 (2017).
[26] See Supplemental Material at http://link.aps.org/supplemental/10.1103/PhysRevLett.129.206801 for the relaxed atomic positions in the device region.
[27] S. Leitherer, N. Papior, and M. Brandbyge, Current-induced atomic forces in gated graphene nanoconstrictions, Phys. Rev. B **100**, 035415 (2019).
[28] M. Di Ventra and S. T. Pantelides, Hellmann-Feynman theorem and the definition of forces in quantum time-dependent and transport problems, Phys. Rev. B **61**, 16207 (2000).
[29] K. H. Bevan, H. Guo, E. D. Williams, and Z. Zhang, First-principles quantum transport theory of the enhanced wind force driving electromigration on Ag(111), Phys. Rev. B **81**, 235416 (2010).
[30] K. H. Bevan, W. Zhu, G. M. Stocks, H. Guo, and Z. Zhang, Local fields in conductor surface electromigration: A first-principles study in the low-bias ballistic limit, Phys. Rev. B **85**, 235421 (2012).
[31] R. Landauer, Spatial variation of currents and fields due to localized scatterers in metallic conduction, IBM J. Res. Dev. **1**, 223 (1957).
[32] N. Papior, T. Gunst, D. Stradi, and M. Brandbyge, Manipulating the voltage drop in graphene nanojunctions using a gate potential, Phys. Chem. Chem. Phys. **18**, 1025 (2016).
[33] H. J. Kulik, Perspective: Treating electron over-delocalization with the DFT + U method, J. Chem. Phys. **142**, 240901 (2015).
[34] A. Bajaj and H. J. Kulik, Eliminating delocalization error to improve heterogeneous catalysis predictions with molecular DFT + U, J. Chem. Theory Comput. **18**, 1142 (2022).
[35] Z.-F. Liu, D. A. Egger, S. Refaely-Abramson, L. Kronik, and J. B. Neaton, Energy level alignment at molecule-metal interfaces from an optimally tuned range-separated hybrid functional, J. Chem. Phys. **146**, 092326 (2017).